Surrogate-Based Multi-Objective Optimization of HDH Desalination Systems Using Artificial Neural Networks

Karim M. Ali[1], Omar H. Khater[2], and Mohammad Abido[3,4]

[1]Department of Mechanical Engineering, [2]Department of Computer Engineering, [3]Department of Electrical Engineering,
[4]Interdisciplinary Research Center for Sustainable Energy Systems (IRC-SES),
King Fahd University of Petroleum and Minerals (KFUPM), Dhahran, Saudi Arabia

***Abstract*—Humidification–dehumidification (HDH) desalination is a promising low-temperature option for freshwater production, but accurate performance prediction across different extraction layouts is computationally expensive due to strongly coupled heat and mass transfer effects. To enable rapid design space exploration, this work develops artificial neural network (ANN) surrogate models for three HDH configurations: zero extraction, single extraction, and double extraction. The ANN surrogates are then integrated with the Non-Dominated Sorting Genetic Algorithm II (NSGA-II) to solve a bi-objective optimization problem that maximizes the gain output ratio (GOR) while minimizing a representative dehumidifier area metric. Across the three configurations, the trained ANN models achieve high predictive performance, with R^2 values close to unity. Pareto front analysis shows a clear improvement in the GOR area trade-off as the number of extraction stages increases. Overall, double extraction provides the most favorable balance between water productivity and dehumidifier size among the studied layouts.**

I. Introduction & Background

Inadequate access to freshwater has become one of the most urgent global challenges of the twenty-first century. Rapid population growth, industrialization, and the impacts of climate change are intensifying pressure on already stressed water resources. Recent assessments by UNESCO and UN-Water indicate that roughly half of the world's population experiences severe water scarcity for at least part of the year, and a substantial fraction lives in regions facing chronically high water stress [1], [2].

Conventional freshwater resources alone are therefore insufficient to meet the projected demand, motivating a growing reliance on technologies that convert saline or brackish water into potable water. Among commercially deployed technologies, reverse osmosis (RO), multi-stage flash (MSF), and multi-effect distillation (MED) are the most prevalent [3]. However, these processes are generally energy-intensive and require high-grade thermal or electrical energy, limiting their suitability for decentralized applications and integration with low-temperature renewable heat sources. In this context, humidification–dehumidification (HDH) desalination has been recognized as a promising low-temperature and low-pressure alternative that can be driven by solar energy or waste heat and is well suited to small- and medium-scale, distributed installations [4].

HDH desalination is inspired by the natural hydrological cycle. In a typical HDH system, a stream of air is brought into contact with warm saline water in a humidifier, where it becomes increasingly humidified. The moist air is then cooled in a dehumidifier, causing water vapor to condense and produce freshwater. Multiple system configurations have been proposed, including zero-extraction, single-extraction, and double-extraction arrangements. These configurations differ in how intermediate humid air streams are withdrawn and recirculated to enhance heat recovery and improve overall thermal efficiency. As a result, the choice of configuration strongly influences evaporation rate, heat recovery, gain output ratio (GOR), and specific energy consumption.

Despite the conceptual simplicity of HDH systems, rigorous performance prediction is challenging. The underlying behavior is highly nonlinear due to the simultaneous occurrence of coupled heat- and mass-transfer phenomena in the humidifier and dehumidifier. Developing accurate physics-based models for different HDH configurations is therefore computationally demanding and time-consuming, particularly when such models are to be embedded in design or optimization routines. Artificial neural networks (ANNs) have proven effective for system identification of nonlinear dynamical systems and offer a flexible data-driven alternative for capturing complex input–output relationships without requiring explicit formulation of governing equations, as highlighted in previous studies [5], [6].

In this work, an ANN-based system identification approach is proposed for modeling three HDH desalination configurations: zero extraction, single extraction, and double extraction. The trained ANN models are used as surrogate models to rapidly predict key performance indicators, particularly the gain output ratio and the dehumidifier surface area, which is directly related to capital cost. Based on these surrogate models, the Non-Dominated Sorting Genetic Algorithm II (NSGA-II) is employed to perform multi-objective optimization of the three systems. NSGA-II is a widely used evolutionary algorithm that efficiently generates a diverse set of Pareto-optimal solutions for conflicting design objectives [7]. The objectives considered here are to maximize the gain-to-output ratio and minimize the dehumidifier area.

The main contributions of this study are therefore threefold:

- The development of ANN-based surrogate models that obviate the need for repeated solution of detailed thermodynamic models.
- The application of NSGA-II to obtain Pareto-optimal HDH designs balancing thermodynamic efficiency and component size.
- A comparative performance investigation of zero-extraction, single-extraction, and double-extraction HDH configurations.

II. Literature Review

Humidification–dehumidification (HDH) desalination has been widely investigated as a low-temperature, low-pressure alternative to conventional thermal and membrane desalination technologies. Several reviews and design studies show that HDH is particularly attractive for small- and medium-scale applications, and for coupling with solar or other low-grade heat sources, because of its relatively simple equipment and its ability to operate with modest temperatures and pressures [8], [9]. Within this context, the gained output ratio (GOR) and the energy effectiveness of heat-and-mass exchangers have been established as primary performance indicators for HDH cycles, enabling meaningful comparison with traditional processes such as multi-stage flash (MSF), multi-effect distillation (MED), and reverse osmosis (RO) [4].

A substantial body of work has focused on understanding how different HDH configurations influence performance. Early thermodynamic analyses examined closed-water/open-air and closed-air/open-water cycles and proposed several high-performance layouts incorporating multiple extractions and injections of humid air to thermodynamically balance the system and enhance heat recovery [9]. Subsequent studies developed more detailed design procedures for thermodynamically balanced HDH cycles, including zero-, single-, and double-extraction configurations, using temperature–enthalpy diagrams and enthalpy pinch analysis to identify near-reversible operating conditions and size humidifiers and dehumidifiers to meet specified design requirements [10].

Related work on the impact of extraction demonstrated that properly selected extraction profiles can markedly increase GOR and reduce equipment size, though at the expense of additional design and control complexity [11]. More recent parametric and experimental investigations confirm that the extraction ratio, air and water flow rates, and top-cycle temperature strongly affect yield and energy efficiency in HDH plants, both with and without mass extraction [12].

Accurate modeling of HDH systems remains challenging due to the strong coupling between heat and mass transfer in both the humidifier and the dehumidifier. Classical mechanistic models typically rely on distributed mass and energy balances along packed columns, together with empirical correlations for heat- and mass-transfer coefficients. These models have been successfully used for conceptual design, sensitivity analysis, and configuration screening, but they can be computationally intensive when large design spaces or many operating points must be explored [9], [10].

To address these limitations, data-driven approaches based on artificial neural networks (ANNs) have been introduced in desalination modeling. In membrane desalination, several studies have shown that ANNs can accurately predict permeate flux, salt rejection, and specific energy consumption from operating and design variables, often outperforming traditional response-surface methods and enabling multivariate sensitivity analysis and optimization [13]. Building on this experience, ANN-based models have recently been developed specifically for HDH systems. One contribution proposed an ANN surrogate to rate and size a thermodynamically balanced HDH cycle with zero, single, and double air extractions, showing that the network can reliably predict GOR and equipment size over a broad operating range and significantly reduce the computational effort compared with detailed thermodynamic solvers [14].

In parallel with advances in modeling, multi-objective optimization has become an essential tool for the design of energy and water systems. The Non-Dominated Sorting Genetic Algorithm II (NSGA-II) has been widely adopted to explore trade-offs between thermodynamic efficiency, cost, and environmental impact. In desalination, NSGA-II has been applied to forward osmosis units, integrated MED–TVC plants, and hybrid cogeneration schemes combining power and RO or MSF, typically balancing exergy efficiency, freshwater cost, and component-level performance indicators [15], [16]. More recently, intelligent frameworks have coupled high-fidelity ANN surrogates with NSGA-II to optimize complex polygeneration systems that include desalination stages, thereby accelerating the search for Pareto-optimal solutions while maintaining good prediction accuracy [17]. These works highlight the potential of ANN-assisted NSGA-II to handle strongly nonlinear, multi-parameter design spaces.

Despite these developments, comparatively few studies combine ANN-based system identification with NSGA-II in the specific context of HDH desalination, and those that do often focus on a single configuration or a limited set of objectives. The literature on thermodynamically balanced HDH cycles with zero, single, and double extractions primarily emphasizes detailed physical modeling and deterministic design procedures, while recent ANN-based studies demonstrate predictive capability but stop short of comprehensive multi-objective optimization of competing layouts [10], [14].

Moreover, most optimization efforts in desalination prioritize efficiency and cost at the plant level, rather than simultaneously considering GOR and key sizing parameters such as dehumidifier surface area. In contrast, the present work develops ANN-based surrogate models for three HDH configurations (zero, single, and double extraction) and integrates them with NSGA-II to obtain Pareto-optimal solutions that explicitly balance GOR and dehumidifier area, thereby extending existing modeling and optimization frameworks and providing a unified basis for comparing alternative HDH layouts.

III. Proposed Methodology

A. Overview

This work performs multi-objective design optimization of humidification–dehumidification (HDH) desalination configurations using a surrogate-based workflow. Three configurations are considered: *zero extraction*, *single extraction*, and *double extraction*. For each configuration, an artificial neural network (ANN) surrogate is used to approximate the mapping from operating inputs to system performance outputs. A multi-objective evolutionary algorithm (NSGA-II) is then applied to compute Pareto-optimal trade-offs between productivity and a representative area/cost metric.

This section first formulates the multi-objective optimization problem by defining the decision variables, objectives, and bounds. It then describes the solution methodology, which is based on ANN surrogate modeling and NSGA-II optimization.

B. Data, Inputs, and Outputs

For each configuration $c \in \{0, 1, 2\}$ (zero, single, double extraction), a dataset $\mathcal{D}^{(c)} = \{(\mathbf{x}_i, \mathbf{y}_i)\}_{i=1}^{N}$ is provided, where the input vector is

$$\mathbf{x} = \left[T_{\min},\, T_{\max},\, \Psi\right]^{\top}, \tag{1}$$

with $T_{\min}$ and $T_{\max}$ in °C and Ψ in kJ/kg.

The output vector $\mathbf{y}$ contains the gain output ratio (GOR) and additional state and performance quantities. For optimization, two key outputs are used:

- Productivity: GOR (to be maximized).
- Representative area/cost metric A (to be minimized). In the present implementation, $A = \mathrm{UA}/m_A$ for zero extraction and $A = U_1 a_1/m_{A1}$ for single and double extraction.

Other stage-wise area terms (e.g., $U_2 a_2/m_{A2}$, $U_3 a_3/m_{A3}$) are computed for reporting but are not included as objectives to avoid redundancy when these quantities are strongly correlated.

C. Surrogate Modeling (ANN)

For each configuration, an ANN surrogate $\widehat{\mathbf{y}} = \mathcal{M}^{(c)}(\mathbf{x})$ is used to predict outputs in physical units. Prior to training and inference, input and output variables are standardized using statistics computed on the training subset:

$$\tilde{\mathbf{x}} = \frac{\mathbf{x} - \boldsymbol{\mu}_x}{\boldsymbol{\sigma}_x}, \tag{2}$$

$$\tilde{\mathbf{y}} = \frac{\mathbf{y} - \boldsymbol{\mu}_y}{\boldsymbol{\sigma}_y}. \tag{3}$$

During inference, the ANN produces $\tilde{\mathbf{y}}$ and the prediction is mapped back to original units via

$$\widehat{\mathbf{y}} = \tilde{\mathbf{y}} \odot \boldsymbol{\sigma}_y + \boldsymbol{\mu}_y, \tag{4}$$

where $\odot$ denotes element-wise multiplication.

Model parameters are loaded from configuration-specific weight files. The ANN architecture is matched exactly to the trained model for each configuration (e.g., an input layer with size 3, a configuration-dependent hidden layer, and an output layer sized to the number of outputs for that dataset).

The ANN models are trained using a mean squared error (MSE) loss function. Optimization is performed using the Adam optimizer with a learning rate of 0.001. A hyperbolic tangent (tanh) activation function is used in the hidden layer. Input and output variables are standardized using a StandardScaler to improve training stability.

The dataset is randomly shuffled and split into training (70%), validation (15%), and testing (15%) subsets using a fixed random seed to ensure reproducibility. No explicit regularization techniques are applied, and model generalization is ensured through validation-based model selection.

D. Decision Variables and Bounds

To reduce dimensionality and align with the experimental design, $T_{\min}$ is fixed to a specified value $T^{\star}_{\min}$ (e.g., 20°C, 30°C, or 40°C). The decision vector is

$$\mathbf{z} = \left[T_{\max},\, \Psi\right]^{\top}. \tag{5}$$

Lower and upper bounds for $\mathbf{z}$ are obtained from the subset of the dataset with $T_{\min} \approx T^{\star}_{\min}$:

$$\mathbf{z} \in [\mathbf{z}_{\ell}, \mathbf{z}_u], \tag{6}$$

ensuring that the optimizer searches within the data-supported operating domain.

E. Multi-Objective Optimization Problem

For each configuration and fixed $T^{\star}_{\min}$, the optimization problem is formulated as

$$\min_{\mathbf{z}} \quad \mathbf{f}(\mathbf{z}) = \begin{bmatrix} f_1(\mathbf{z}) \\ f_2(\mathbf{z}) \end{bmatrix} = \begin{bmatrix} -\widehat{\mathrm{GOR}}(\mathbf{z}) \\ \widehat{A}(\mathbf{z}) \end{bmatrix}, \tag{7a}$$

$$\text{s.t.} \quad \mathbf{z}_{\ell} \le \mathbf{z} \le \mathbf{z}_u, \tag{7b}$$

where $\widehat{\mathrm{GOR}}(\mathbf{z})$ and $\widehat{A}(\mathbf{z})$ are ANN predictions evaluated at $\mathbf{x} = [T^{\star}_{\min},\, T_{\max},\, \Psi]^{\top}$.

To avoid non-physical negative area predictions that can arise from surrogate extrapolation or regression error, the representative area metric can be enforced as non-negative during evaluation using

$$\widehat{A} \leftarrow \max\{0, \widehat{A}\}. \tag{8}$$

This yields physically meaningful objective values while preserving the overall Pareto trade-off structure.

F. NSGA-II Settings

The bi-objective problem is solved using NSGA-II. Each run is parameterized by a population size N_{pop} and a maximum number of generations N_{gen} (e.g., $N_{\mathrm{pop}} = 150$ and $N_{\mathrm{gen}} = 10$ or 15), with a fixed random seed for reproducibility. The algorithm returns a set of candidate solutions along with objective and constraint values.

G. Pareto Front Extraction and Reporting

After optimization, the *true* Pareto set is then extracted from points using non-dominated sorting (i.e., retaining only solutions that are not dominated in the objective space). For interpretability, two visualizations are produced:

- GOR versus A (maximize productivity, minimize area/cost),
- $1/\mathrm{GOR}$ versus A (both axes interpreted as costs to be minimized).

To facilitate concise reporting, the Pareto front can be downsampled to K representative solutions (e.g., $K = 30$) selected approximately uniformly along the sorted front. For each selected Pareto design, the full set of ANN-predicted outputs is exported to a CSV file. Output artifacts (CSV and figures) are named to explicitly encode the configuration ($c \in \{0, 1, 2\}$) and fixed temperature $T^{\star}_{\min}$ to ensure traceability across experimental runs.

IV. Experimental Setup

We use three datasets provided/derived from the synthetic data generation procedure of [14]. The data are generated by solving a physics-based numerical model of a closed-air open-water, water-heated humidification–dehumidification (CAOW-WH HDH) desalination system (implemented in EES). Each sample corresponds to a set of operating conditions and the associated performance and sizing outputs computed from the underlying thermodynamic model.

The synthetic dataset is generated by randomly sampling the input variables within their specified ranges, ensuring uniform coverage of the operating domain. The physics-based EES model is used to generate the corresponding outputs, which serve as the ground truth for training and evaluation.

The dataset is randomly divided into training (70%), validation (15%), and testing (15%) subsets to ensure proper model generalization and unbiased performance evaluation.

A. Input variables.

Following [14], we consider three key operating inputs: minimum seawater temperature $T_{w,0}$, maximum (heating) seawater temperature $T_{w,2}$, and enthalpy pinch Ψ. The operating ranges are: $T_{w,0} \in [20, 40]\,^{\circ}\mathrm{C}$, $T_{w,2} \in [60, 80]\,^{\circ}\mathrm{C}$, and $\Psi \in [1, \Psi_{\mathrm{cr}}]$ (where Ψ_{cr} depends on the extraction configuration). The number of extractions is handled by splitting the data into three separate datasets (zero, single, and double extraction).

B. Output variables.

The task is formulated as a multi-output regression. The number of outputs depends on the number of extraction stages: 10 outputs for the zero-extraction case, 18 outputs for the single-extraction case, and 26 outputs for the double-extraction case. The summary of the datasets used in this study is presented in Table I.

TABLE I
DATASET SUMMARY

Dataset	# Solutions	# Inputs	# Outputs
ANN_Data_Zero_Extraction	17,162	3	10
ANN_Data_Single_Extraction	9,000	3	18
ANN_Data_Double_Extraction	9,000	3	26

In addition, separate artificial neural network models are trained for each extraction configuration. The adopted network architectures are 3–28–10, 3–36–18, and 3–40–26 for the zero-, single-, and double-extraction cases, respectively. The number of hidden neurons is selected based on minimizing the validation mean squared error to balance model accuracy and generalization.

V. Results and Discussions

A. ANN Results

TABLE II
ANN PREDICTIVE PERFORMANCE FOR DIFFERENT HDH EXTRACTION CONFIGURATIONS.

Configuration	R^2
Zero Extraction	0.9814
Single Extraction	0.9979
Double Extraction	0.9983

As shown in Table II, the proposed ANN surrogate models achieve high predictive performance across all HDH configurations. The zero-extraction model demonstrates reliable performance, with an R^2 value of 0.9814. The performance further improves in the single- and double-extraction cases, with coefficients of determination approaching unity. This trend indicates that the ANN models effectively capture the increasing system complexity introduced by additional extraction stages, validating their suitability for subsequent multi-objective optimization.

B. NSGA-II Results

The trained ANN models were coupled with NSGA-II to explore the trade-off between thermodynamic performance and component size for the zero-, single-, and double-extraction HDH configurations. The two objectives were the gain output ratio (GOR) and the total dehumidifier area A. For graphical clarity and to cast both objectives as minimization problems, the Pareto fronts are reported in terms of the inverse GOR, $1/\mathrm{GOR}$, versus A. The resulting fronts for each configuration are shown in Figs. 1–3, while Fig. 4 superimposes the three curves using power–law fits. For each front, a representative compromise solution is selected near the "knee" of the curve, corresponding to operating conditions defined by the optimal maximum temperature $T_{\max}$ and enthalpy-pinch parameter Ψ.

1) Zero-extraction configuration: The Pareto-optimal solutions for the zero-extraction configuration are reported in Fig. 1. The front spans dehumidifier areas from approximately 0.5 to 7.5 m^2, with $1/\mathrm{GOR}$ decreasing from values larger than 8 to about 0.1. This behavior reflects the strong trade-off between GOR and area: designs with very small area exhibit poor thermodynamic performance, whereas increasing A enhances GOR but with diminishing returns in the high-area region.

A compromise solution is selected near the knee of the front at $\mathrm{GOR} = 0.70$ and $A = 1.33$ m^2 . At this point, the ANN–NSGA-II framework identifies a combination of $T_{\max} = 62$ °C and $\Psi = 60.8$ (subject to the enthalpy-pinch constraint) that avoids the very low-GOR region while keeping the required The dehumidifier area is relatively modest. This solution is adopted as the reference point for the zero-extraction layout in the subsequent comparison.

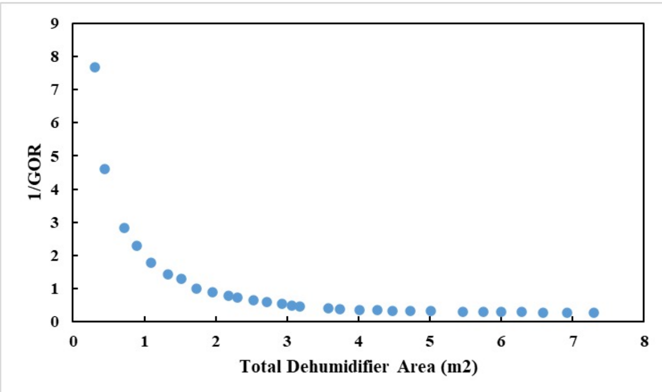

Fig. 1. Zero-Extraction system pareto front

2) Single-extraction configuration: Fig. 2 shows the Pareto front obtained for the single-extraction configuration. Compared with the zero-extraction case, the curve is shifted markedly towards lower $1/\mathrm{GOR}$ values for overlapping ranges of A, indicating that the introduction of one extraction stage enables substantially higher GOR for a given dehumidifier area. The front extends from $A = 4$ to 15 m^2, while $1/\mathrm{GOR}$ drops from about 0.4 to below 0.08.

The compromise point for this configuration is located at $\mathrm{GOR} = 5.71$ and $A = 7.97$ m^2 , corresponding to $T_{\max} = 60.4$ °C and $\Psi = 8.0$. Relative to the zero-extraction compromise design, GOR increases by a factor of approximately 8.1, while the required dehumidifier area increases by a factor of about 6.0. This illustrates the cost of achieving much higher water productivity when only one extraction position is available: the thermodynamic gains are substantial, but they come at the expense of a significant increase in heat-transfer surface.

3) Double-extraction configuration: The Pareto-optimal solutions for the double-extraction configuration are depicted in Fig. 3. The front covers areas from approximately 8 to 20 m^2, with $1/\mathrm{GOR}$ varying smoothly from about 0.15 to 0.035. For a large portion of this range, the curve lies below the single-extraction front, showing that double extraction can simultaneously provide higher GOR and comparable or even smaller area for certain operating points.

The selected compromise solution for the double-extraction layout occurs at $\mathrm{GOR} = 14.56$ and $A = 13.15$ m^2, with $T_{\max} = 60.0$ °C and $\Psi = 3.88$. Compared with the single-

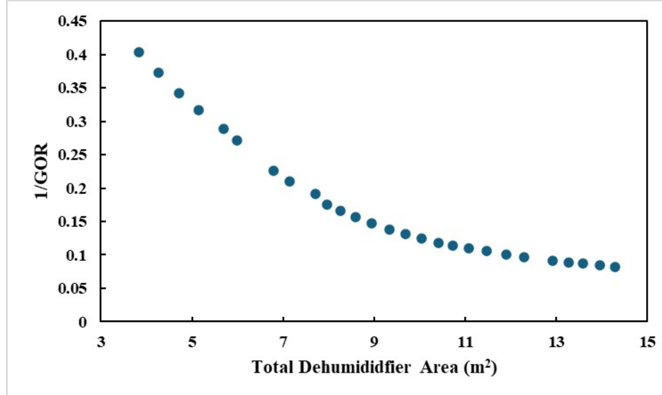

Fig. 2. Single-Extraction system pareto front

extraction compromise point, GOR increases by a factor of about 2.6, whereas the area grows by only 66.5%. When compared directly to the zero-extraction compromise solution, the double-extraction layout delivers roughly 21 times higher GOR at the expense of about 10 times larger dehumidifier area. These results highlight the strong leverage offered by multiple extraction stages on the thermodynamic efficiency of the HDH cycle.

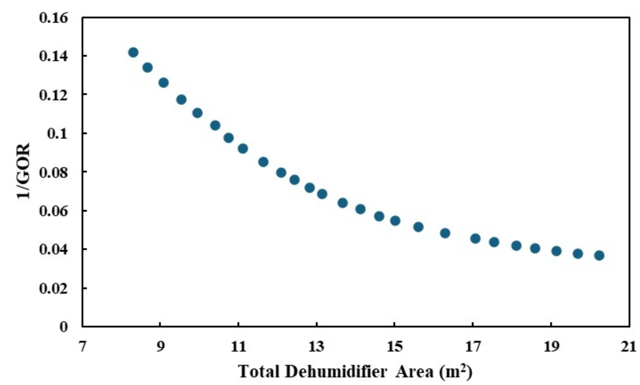

Fig. 3. Double-extraction system Pareto front

4) Comparison of extraction layouts: To better visualize the relative performance of the three layouts, Fig. 4 superimposes the corresponding Pareto fronts, together with power–law correlations of the form

$$\frac{1}{\mathrm{GOR}} = aA^b, \tag{9}$$

fitted to the NSGA-II solutions. For the zero-, single-, and double-extraction configurations, the parameters are $(a, b) = (1.593, -0.979)$, $(2.6173, -1.308)$, and $(19.316, -2.012)$, respectively, with coefficients of determination R^2 in the range 0.97–0.99. These high R^2 values indicate that Eq. (9) provides an accurate and compact representation of the numerical Pareto sets, suitable for use as design curves.

The combined plot clearly shows a progressive downward shift of the fronts as the number of extraction stages in-

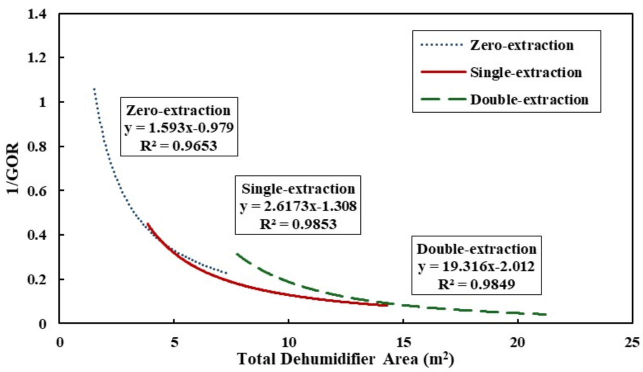

Fig. 4. Design curve using pareto fronts

creases. For a given dehumidifier area, single extraction always outperforms zero extraction, and double extraction provides the lowest $1/\mathrm{GOR}$ over most of the common area range. In other words, the additional extraction stages enhance internal heat recovery and allow the system to operate closer to the thermodynamic optimum. In small areas, the zero-extraction layout remains attractive in terms of compactness but suffers from low GOR. As A increases beyond about 6–8 m^2, the single-extraction curve lies strictly below the zero-extraction one, while the double-extraction curve approaches the lowest region of the $(1/\mathrm{GOR}, A)$ plane.

When the three compromise points are considered together, a clear trend emerges: moving from zero to single extraction yields a large gain in GOR with a substantial but acceptable increase in area, and adding a second extraction stage further improves GOR at a relatively moderate additional area penalty. The double-extraction compromise solution therefore, offers the most favorable balance between water productivity and dehumidifier size among the configurations studied, suggesting that multiple extraction stages are a promising strategy for the design of high-performance HDH desalination systems.

VI. Conclusion

This study presented a surrogate-based framework for multi-objective optimization of HDH desalination systems with zero, single, and double air extraction. ANN models were used to approximate the mapping from operating conditions to key performance indicators, enabling fast evaluation during NSGA-II optimization of two competing objectives: maximizing GOR and minimizing a representative dehumidifier area. The ANN surrogates achieved strong evaluation metrics across all configurations, supporting their use for optimization. The resulting Pareto fronts reveal a consistent improvement in the GOR–area trade-off with additional extraction stages: single extraction outperforms zero extraction over overlapping area ranges, while double extraction provides the lowest $1/\mathrm{GOR}$ over most of the common domain. Comparing representative compromise solutions further confirms this trend, with double extraction delivering the highest productivity at a moderate additional area penalty relative to single extraction. These findings suggest that incorporating multiple extraction stages can significantly enhance HDH thermodynamic performance while maintaining a practical trade-off in component sizing.

VII. Acknowledgment

The authors would like to acknowledge the support provided by the Interdisciplinary Research Center for Sustainable Energy Systems, King Fahd University of Petroleum and Minerals, Saudi Arabia.

References

[1] UNESCO and UN-Water, "Un world water development report 2024: Water for prosperity and peace," Tech. Rep., 2024.

[2] UN-Water, "Progress on level of water stress – 2024 update," UN-Water, Tech. Rep., 2024.

[3] D. Curto, V. Franzitta, and A. Guercio, "A review of the water desalination technologies," *Applied Sciences*, vol. 11, no. 2, 2021. [Online]. Available: https://www.mdpi.com/2076-3417/11/2/670

[4] R. Santosh, H.-S. Lee, and Y.-D. Kim, "A comprehensive review on humidifiers and dehumidifiers in solar and low-grade waste heat powered humidification-dehumidification desalination systems," *Journal of Cleaner Production*, vol. 347, p. 131300, 2022. [Online]. Available: https://www.sciencedirect.com/science/article/pii/S0959652622009295

[5] G. Pillonetto, A. Aravkin, D. Gedon, L. Ljung, A. H. Ribeiro, and T. B. Schön, "Deep networks for system identification: A survey," *Automatica*, vol. 171, p. 111907, 2025.

[6] R. Eischens, T. Li, G. Vogl, Y. Cai, and Y. Qu, "State space neural network with nonlinear physics for mechanical system modeling," *Reliability Engineering & System Safety*, 2025.

[7] K. Deb, A. Pratap, S. Agarwal, and T. Meyarivan, "A fast and elitist multiobjective genetic algorithm: Nsga-ii," *IEEE Transactions on Evolutionary Computation*, vol. 6, no. 2, pp. 182–197, 2002.

[8] J. H. L. V, "Humidification–dehumidification desalination," Rohsenow Kendall Heat Transfer Laboratory, Massachusetts Institute of Technology, Tech. Rep., 2019, preprint, available via MIT DSpace.

[9] G. P. Narayan, M. H. Sharqawy, J. H. L. V, and S. M. Zubair, "Thermodynamic analysis of humidification–dehumidification desalination cycles," *Desalination and Water Treatment*, vol. 16, pp. 339–353, 2010.

[10] M. S. Elzayed, M. A. M. Ahmed, N. A. A. Qasem, M. A. Antar, and S. M. Zubair, "A design procedure to size thermodynamically-balanced humidification–dehumidification desalination systems," *Energy Conversion and Management*, vol. 224, p. 113357, 2020.

[11] J. A. Miller, J. H. L. V, and S. M. Zubair, "Impact of extraction on a humidification–dehumidification desalination system," *Desalination*, vol. 313, pp. 87–96, 2013.

[12] A. Tiwari and A. Kumar, "Energy, exergy, environmental, and economic (4e's) analysis of a solar driven humidification–dehumidification desalination system: An experimental investigation," *Thermal Science and Engineering Progress*, vol. 47, p. 102354, 2024.

[13] N. R. authors, "Optimizing reverse osmosis desalination from brackish waters using response surface methodology and artificial neural network," *Journal of Industrial and Engineering Chemistry*, 2024, rO desalination modeling with ANN and RSM.

[14] M. Ahmed, N. A. Qasem, M. Abido, M. A. Antar, and S. M. Zubair, "On using artificial neural network models for a thermodynamically-balanced humidification-dehumidification system: design and rating analysis," *Energy Conversion and Management: X*, vol. 18, p. 100380, 2023.

[15] S. Sigue, S. Abderafi, and T. Bounahmidi, "Multi-objective optimization of a forward osmosis process for desalination using a non-dominated sorting genetic algorithm," *Journal of Water Process Engineering*, vol. 58, p. 104804, 2024.

[16] M. Imandoust, S. T. K. Alghorayshi, R. Zahedi, A. Aslani, and M. Q. Khanqah, "Multi-objective optimization of hybrid solar–wind msf–ro cogeneration desalination systems using nsga-ii to enhancing energy efficiency, cost reduction and sustainability," *Separation and Purification Technology*, vol. 321, p. 134740, 2025.

[17] M. A. Haghghi, M. Feili, P. Nourani, and A. M. Bahman, "An intelligent nsga-ii-based optimization of a novel biogas-fed oxyfuel gas turbine cycle using co_2 capture option coupled with a multi-heat recovery network and a multi-effect desalination cycle," *Desalination*, vol. 585, p. 118957, 2025.